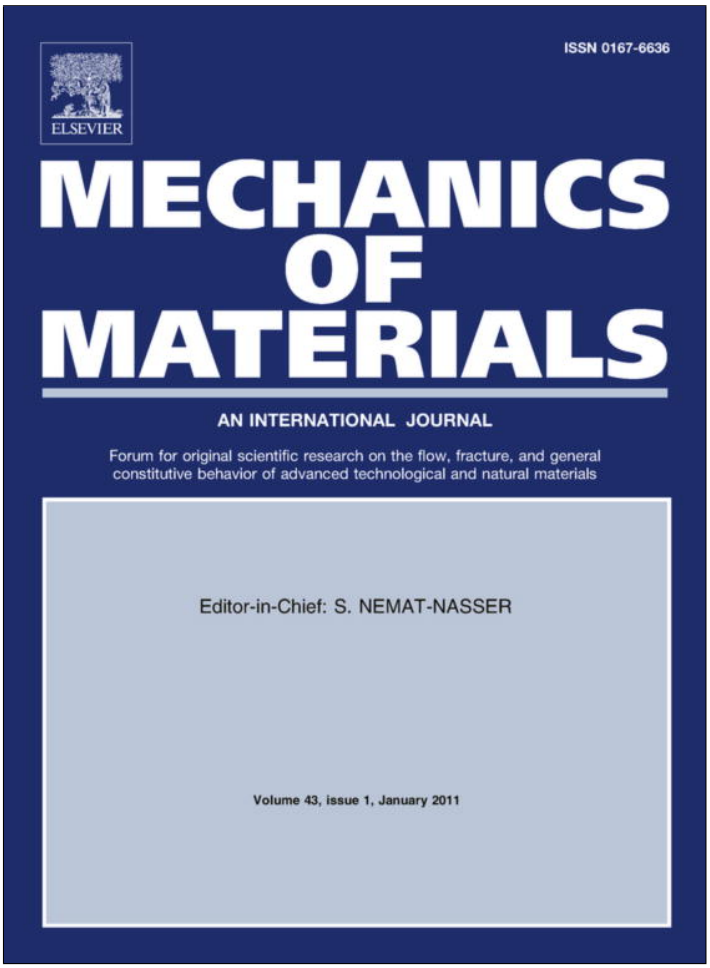

(This is a sample cover image for this issue. The actual cover is not yet available at this time.)

Mechanics of Materials 43 (2011) 476–486

Contents lists available at ScienceDirect

Mechanics of Materials

journal homepage: www.elsevier.com/locate/mechmat

The helical auxetic yarn – A novel structure for composites and textiles; geometry, manufacture and mechanical properties

M.R. Sloan *, J.R. Wright, K.E. Evans

College of Engineering, Mathematics and Physical Sciences, University of Exeter, UK

ARTICLE INFO

Article history:
Received 4 May 2010
Received in revised form 5 January 2011
Available online 1 June 2011

Keywords:
Poisson's ratio
Auxetic
Yarn
Fibres
Mechanical properties

ABSTRACT

This paper introduces a novel fibre structure known as the helical auxetic yarn (HAY). The geometry of the yarn is defined and the manufacturing process described. A range of HAYs have been manufactured that vary the geometric properties of the structure. A systematic study of the yarns has been completed to evaluate the effect on the auxetic behaviour of the geometry. We also characterise the component fibres and yarns and discuss the influence of geometric and material effects on the observed Poisson's ratio of the yarns.

It can be shown that the starting wrap angle of the yarn has the greatest effect on auxetic behaviour both in terms of magnitude and the strain range over which it may be observed.

The maximum negative Poisson's ratio observed for a yarn manufactured from conventionally available monofilaments with positive Poisson's ratio is −2.7.

1. Introduction

Negative Poisson's ratio or auxetic (Lakes, 1987; Evans et al., 1991) materials have received considerable attention over the last 3 decades due to their counter intuitive behaviour of expanding laterally when subjected to a tensile load and vice versa under compression. This behaviour can enhance fundamental bulk properties such as the shear modulus, indentation resistance, fracture toughness and synclastic curvature (Evans and Alderson, 2000). Auxetic behaviour has been demonstrated in materials ranging from naturally occurring single crystals (Williams et al., 2007) and cubic metals (Baughman et al., 1998), to biological materials such as skin (Lees et al., 1991; Frohlich et al., 1994) bone (Williams and Lewis, 1982) and synthetic materials such as foams (Chan and Evans, 1997, 1998), honeycomb structures (Gaspar et al., 2005) and composites (Theiocaris et al., 1997; Evans et al., 2004; Hilton et al., 2008; Kocer et al., 2009). Synthesised auxetic materials are highly attractive as this allows mechanical properties to be carefully tailored for specific applications by controlling the material structure.

The fundamental mechanism behind auxetic behaviour and also the length scale over which it is observed varies between materials. Single crystal arsenic (Gunton and Saunders, 1972) and zeolites (Williams et al., 2007) demonstrate auxetic behaviour as a result of molecular bond rotation. Synthetic polymer foams (Lakes, 1987; Chan and Evans, 1997, 1998) show an auxetic effect at strains 6 orders of magnitude greater as a result of an internal re-entrant rib structure – introduced during manufacture – increasing the apparent volume of the material.

Caddock and Evans (1989) demonstrated that highly anisotropic expanded PTFE samples were auxetic by changing the material microstructure through sintering, demonstrating the application to other polymeric materials. The process was repeated using Ultra-high molecular weight polyethylene (Alderson et al., 2000), nylon (Alderson et al., 1998), and polypropylene (Pickles et al., 1996). Further developments by Ravirala et al. (2005) produced auxetic fibres by melt spinning PP, PE and nylon,

* Corresponding author. Address: College of Engineering, Mathematics and Physical Sciences, University of Exeter, Harrison Building, North Park Road, Exeter, Devon EX4 4QF, UK. Tel.: +44 (0) 1392 723667; fax: +44 (0) 1392 723616.

E-mail address: m.r.sloan@exeter.ac.uk (M.R. Sloan).

0167-6636/$ - see front matter © 2011 Elsevier Ltd. All rights reserved.
doi:10.1016/j.mechmat.2011.05.003

Nomenclature

A_c	cross section area core fibre	λ	cyclic pitch of wrap fibre
A_w	cross section area wrap fibre	L_G	clamping Gauge length of yarn
A_y	cross section area yarn	L_O	optical gauge length of yarn
D_c	diameter core fibre	L_w	length traced by the centre of the wrap fibre
D_w	diameter wrap fibre	ν_{xy}	Poisson's ratio
D_y	diameter (effective) of yarn	θ	wrap fibre angle
ε_x	lateral engineering strain	V_c	linear speed crosshead
ε_y	longitudinal engineering strain	v_c	linear feed rate of core fibre (ms^{-1})
f_w	wrap frequency		

proposing their use for enhanced reinforcement in composite materials.

Auxetic fibres provide a potential route to particular auxetic materials as they can be woven into technical textiles opening up further commercial exploitation routes for sporting, medical or defence applications.

Textiles characterised and modelled analytically by Shanahan and Piccirelli (2008) showed auxetic behaviour through the fabric thickness due to a geometric effect as a result of the woven structure. Ugbolue et al. (2007) knitted textiles from nomex and polyester fibres and, by carefully tailoring the textile structure, a Poisson's ratio of −0.6 was measured across the fabric width. Hall et al. (2008) produced carbon nanotube sheets (buckypaper) using a combination of single and multi walled carbon nano-tubes and measured an in-plane Poisson's ratio as low as −0.2 subject to the ratio of single and multi walled tubes. In all cases the auxetic behaviour was attributed to geometric effects.

Auxetic yarns invented by Hook et al. (2006) combined two conventional fibres in a helical arrangement which, when subjected to a tensile strain, exhibited a net increase in the width of the yarn. Miller et al. (2009) provided preliminary test data for one helical auxetic yarn (HAY) system, combined helical auxetic yarns in a simple weave pattern to produce an auxetic textile and used the textile to manufacture and test a low modulus composite.

Helical auxetic yarns form the basis of this paper. We define the geometric parameters of these yarns, describe the manufacture and mechanical characterisation process in detail and also identify the mechanism behind the observed auxetic behaviour. In this paper we undertake a systematic study of monofilament HAYs to determine the parameters of greatest influence to the desired auxetic behaviour.

2. Geometry

A helical auxetic yarn is constructed by combining two fibrous components in a double helix as described by Hook et al. (2006). It has been proposed that the components must possess differing moduli and diameter for the HAY to function optimally. The experimental work in this paper investigates these effects on the auxetic behaviour of the yarns. First the yarn geometry is introduced. A low modulus, initially straight core fibre is uniformly wrapped with a lower diameter and stiffer wrap component as shown in Fig. 1a.

At zero strain the core and wrap fibres are in uniform contact, with the core straight and the wrap helically wound with an internal helix diameter equal to the fibre diameter of the core. Upon application of an axial tensile strain, the wrap fibre straightens and in doing so displaces the core laterally, thus increasing the effective diameter of the system. At full strain the geometry of the core and wrap are reversed with respect to the starting configuration. Fig. 1b shows the HAY at maximum strain.

On removal of the tensile strain, if the wrap and core are elastic, both recover to the initial starting configuration – provided that the elastic limit of the materials has not been exceeded. The auxetic effect can be controlled by selecting fibre diameters, moduli, the initial geometry and also the applied strain.

The benefit of having an auxetic yarn, compared to an intrinsic auxetic fibre lies both in the relative simplicity of the manufacturing process, a simple spinning together of two conventional fibres and the relative ease of tailoring properties.

Fig. 2a defines the geometric parameters associated with a HAY having components of circular cross section. The initial diameters of the core and wrap fibres can be defined as D_c and D_w, respectively. The effective diameter of the yarn is defined by D_y. The cyclic frequency of the wrap fibre can be defined using either the angle θ which subtends the core and wrap or by considering the cyclic pitch of the wrap fibre λ. It is more intuitive to measure and quote the angle θ. However due to practicalities of measurement of the yarns as a function of strain we use the pitch length to calculate the wrap angle. It is also convenient for the manufacturing process to correlate the wrap angle θ to the linear measurement λ.

The cyclic pitch and fibre diameters of a HAY can be described using simple trigonometry. If we take exactly one cycle of a HAY and roll it out on a flat surface, imagining the wrap fibre sticking to the surface as it unravels from the core. This forms a simple right angle triangle as shown in Fig. 2b.

where;

L_w = Length traced by the centre of the wrap fibre (m)
D_c = Diameter of core fibre (m)
D_w = Diameter of wrap fibre (m)
λ = Cyclic pitch of wrap fibre (m)

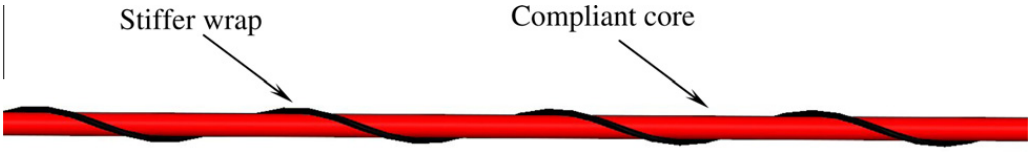

Fig. 1a. HAY at zero strain.

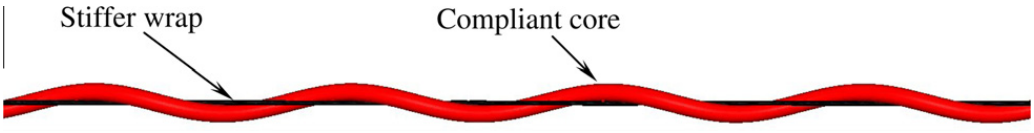

Fig. 1b. Helical auxetic yarn at maximum strain.

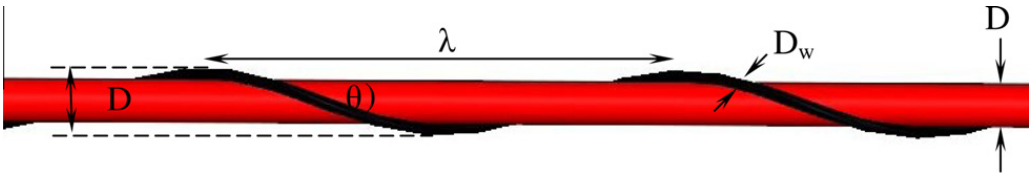

Fig. 2a. Geometric definitions of a monofilament helical auxetic yarn.

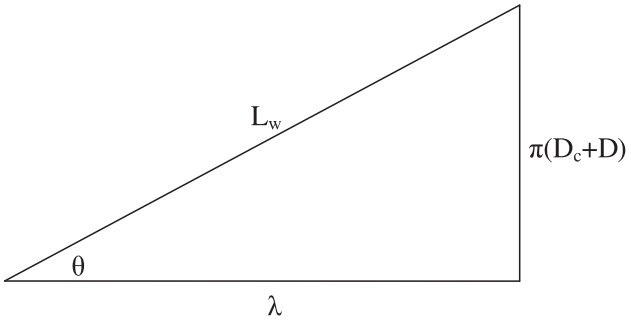

Fig. 2b. Trigonometric relationship of HAY components.

Fig. 3a. HAY at zero strain.

θ = Wrap angle (deg)
D_y = Effective diameter of yarn (m)

From Fig. 2b;

$$\lambda = \frac{\pi(D_c + D_w)}{\tan\theta} \tag{1}$$

Eq. (1) allows the cyclic pitch of a yarn to be calculated for any given fibre diameter pair as a function of the desired wrap angle. The pitch is used in the manufacturing process to accurately produce the required yarn geometry.

The engineering stress in the yarn as a function of the applied longitudinal strain is calculated using the cross

Fig. 3b. Cross section of HAY.

section area of the yarn at zero strain as shown in Fig. 3a. By taking a section through the yarn normal to the applied load, i.e. the major axis of the core fibre at zero strain we can observe a circular core and elliptical wrap as shown in Fig. 3b.

The cross sectional area of the core (A_c) and wrap fibres (A_w) can be calculated using Eqs. (1) and (2) respectively;

$$A_c = \frac{\pi D_c^2}{4} \tag{2}$$

$$A_w = \frac{\pi D_w^2}{\cos\theta} \tag{3}$$

The cross sectional area of the yarn (A_y) is the sum of equations (2) and (3);

$$A_y = A_c + A_w \tag{4}$$

As the yarn is strained and the wrap straightens, its cross section will change from elliptical to circular whereas the reverse is observed for the core which starts circular and tends to an elliptical cross section once activated.

3. Methods

Monofilament core and wrap fibres were sourced from Monofil Technik (www.monofil-technik.de.2007). A polyurethane elastomer trade name TROFIL, nominal 600 μm diameter was selected as the core fibre as it allows large

strain deformations. The wrap fibre was a co-polymer polyamide, trade name Platil in nominal diameters 110 μm, 130 μm and 150 μm. Accurate diameters of core and wrap fibres were obtained by SEM measurements at high magnification. 3 random samples of each monofilament fibre were taken from the spools as supplied by the manufacturer, coated in approximately 5 nm of gold and imaged in a Hitachi S3200 variable pressure SEM using a 20 kV accelerating voltage. Two images were obtained for each sample. Length measurements were taken using the internal calibrated vernier callipers to determine the diameter of the fibres.

Helical auxetic yarns were manufactured using a spinner mechanism designed and built specifically for producing lab-scale lengths of yarns – approximately 10 m. The wrap fibre was used to control the two yarn geometric parameters of interest in this study, the wrap fibre angle and the wrap/core fibre diameter ratio. Yarns of varying wrap angle were manufactured using the 150 μm wrap fibre. A detailed description can be found in Appendix 1.

Fibre and yarn samples were prepared for mechanical testing according to ASTM D3822-07 – tensile properties of single textile fibres (ASTM, 2007). Minor variations between monofilament and HAY samples are discussed below.

Monofilament fibre samples of 70 mm length were taken from bulk spools of fibre and prepared for mechanical testing according to ASTM (2007). Sample ends were secured in 10 mm card tabs using Araldite 2012 to minimise clamp slip. A clamping gauge length L_G of 50 mm was used and an additional gauge length for optical strain measurements L_O marked onto the middle of the fibre such that;

$$L_O = 0.1L_G \pm 5\% \tag{5}$$

Due to the additional geometric complexity of HAYs, the sample gauge length was modified to retain accuracy and consistency throughout the testing.

A sample gauge length L was chosen according to the conditions.

$$50\ \text{mm} \leqslant L_G \quad \text{and} \quad 10\lambda \leqslant L_G \tag{6}$$

This condition was specified by the authors to ensure a minimum number of wrap cycles within a specimen gauge length regardless of yarn geometry and can also be justified by the numerical study by Wright et al. (2010). Gauge length increases as wrap angle decreases so this condition was specified to retain a minimum geometric consistency between yarns.

Tensile measurements were performed using a Lloyd Instruments (www.lloyds-instruments.co.uk) EZ 20 mechanical testing machine using a 50 N load cell and crosshead displacement control via the internal extensometer. The initial clamp separation was set to length using calibrated verniers. The applied load and linear separation of the clamps were recorded using the Nexygen software (www.lloyds-instruments.co.uk) at a data capture frequency of 1 kHz.

Samples were mounted vertically between clamps and secured manually. Monofilaments were tested to failure; HAYs were tested until failure of either the core or wrap, whichever first. The crosshead speed V_c was set as a function of the sample gauge length such that.

$$V_C = 0.1L_G/\ \text{min} \tag{7}$$

This equates to the lowest testing speed specified in ASTM D3822-07 as it allows greater accuracy in image acquisition of the yarns.

A high magnification, non-contact video system controlled by a secondary PC was used to accurately record longitudinal and lateral sample strain. A 4.9 MP digital camera (Edmund Optics EO-5012C USB) acquired images through a variable zoom lens mounted at a fixed working distance of approximately 160 mm from the sample. This allowed simple control over the field of view at a fixed resolution of 2560 × 1920 pixels. The field of view was selected at the start of testing and remained fixed throughout the test. The smallest field of view achievable from the hardware was approximately 8 mm^2, giving the greatest resolution of images and hence accuracy in measurement. Camera lens focus and apertures were set using this condition. A fixed field of view was used throughout the tensile test, and so was increased accordingly to accommodate the accumulated strain within the fibres – both optical and sample gauge lengths. Fig. 4 shows a schematic of the test apparatus. A software macro was added to the Nexygen test procedure, instructing a TTL signal to be sent on the start of the test and at pre-defined regular strain intervals to acquire images throughout the test.

External lighting was employed using an electric lamp and "daylight" bulb. White panels were used around the test set up to reflect and diffuse the light source and so minimise light reflection effects such as halos around the fibres.

Camera hardware was mounted to display the test sample image in a horizontal configuration as shown in Fig. 5 thus exploiting the maximum pixel resolution along the fibre length.

Strains were applied in the positive x direction. This applied to both monofilament and yarn samples.

Yarns were visually inspected before testing to confirm accurate manufacture by inspecting the consistency of

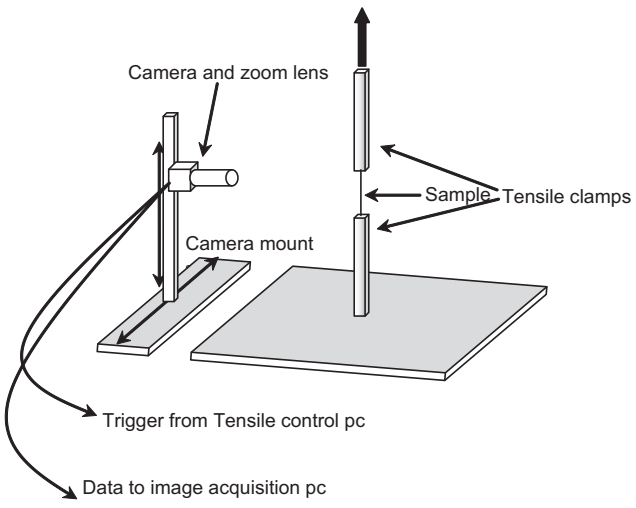

Fig. 4. Image acquisition and tensile testing apparatus.

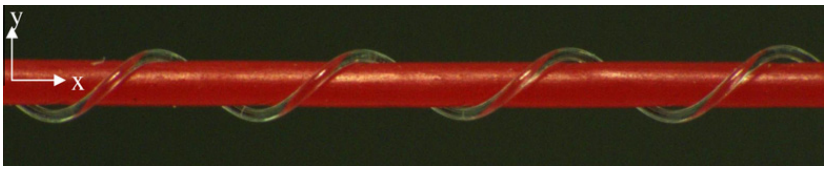

Fig. 5. Configuration of test images.

Fig. 6. Rejected yarn sample.

wrap angle and conformance of the wrap with the core along the entire sample gauge length. Fig. 6 shows a sample rejected before testing due to poor conformance of wrap with the core. Gauge length markers can also be seen on the sample.

Longitudinal and lateral strain measurements were calculated using the images captured during the tensile test at intervals of 0.01 strain. A contrasting sample background was used to enhance the sample edge definition and minimise image compression noise artefacts associated with colour change rather than brightness. Raw bitmap images were converted into JPEG files in Paintshop pro (www.jasc.com) maintaining a 2560×1920 pixel resolution and using the lowest compression factor. Sample dimensions for monofilaments and yarns were calculated using the linear measuring tool in the ImageJ software (Abramoff et al., 2004). All sample and calibration images were processed manually using this method. The length scale was calibrated using the zero strain image for each fibre and the dimensions taken from the SEM images. For monofilaments, longitudinal strain was calculated using the separation of the optical markers and lateral strain using the fibre width.

Image analysis for HAYs was performed in the same manner, however due to the significant change in geometry compared to monofilaments, strain measurement definitions were required. Longitudinal strain was determined by measuring the linear separation of the optical gauge markers. Transverse strain was calculated using the greatest lateral width of the yarn with respect to the axis of the applied tensile load. At low strains this equated to the width measured between peak heights of the wrap fibres. At higher strains when the core has been activated, taking on a sinusoidal wave form, the greatest width is defined by the core.

Poisson's ratio for monofilament fibres and yarns was calculated using engineering strains ε_y and ε_y according to Eq. (4)

$$v_{xy} = -\frac{\varepsilon_y}{\varepsilon_x} \tag{8}$$

Measurement errors were taken as ±2 pixels in both longitudinal and lateral directions. Using the calibrated length scale for individual images, maximum and minimum length measurements were determined and used to calculate the absolute errors in strain measurements and subsequent Poisson's ratio values.

4. Results

4.1. Fibre characterisation

Typical SEM images of the polyurethane elastomer core are shown below in Figs. 7a and b. Width measurements were taken and a median value calculated for each monofilament giving their respective diameters. These diameters were used to calculate the desired pitch length for manufacture of the yarns and the cross sectional areas of the monofilaments.

4.2. Mechanical testing

Fig. 8 shows the engineering stress/strain curve for the monofilament component fibres and their respective helical auxetic yarn with a starting angle of 13°. The polyamide wrap is shown to have a greater modulus and ultimate tensile strength than the elastomeric core fibre. The polyurethane core is able to withstand longitudinal strain 4 times greater than the wrap fibre before failure but demonstrates a much lower tensile stress at failure. Combining the two fibres in a helical arrangement produces a stress strain curve with a higher ultimate tensile stress and elongation at break compared to the component core and wrap fibres, respectively.

Table 1 summarises the mechanical properties of the fibres as shown in Fig. 8. The Young's modulus was calculated using the initial linear elastic region of the engineering stress strain curve. The engineering stress was calculated using circular cross sectional areas for the monofilaments and using Eq. (4) for the yarns.

Table 1
Summary of mechanical properties of core, wrap and yarn.

	PU core	PA wrap	HAY 13°
Young's modulus (MPa)	30	3400	76
Ultimate tensile strength (MPa)	51	789	56
Strain at break (%)	95	17	34

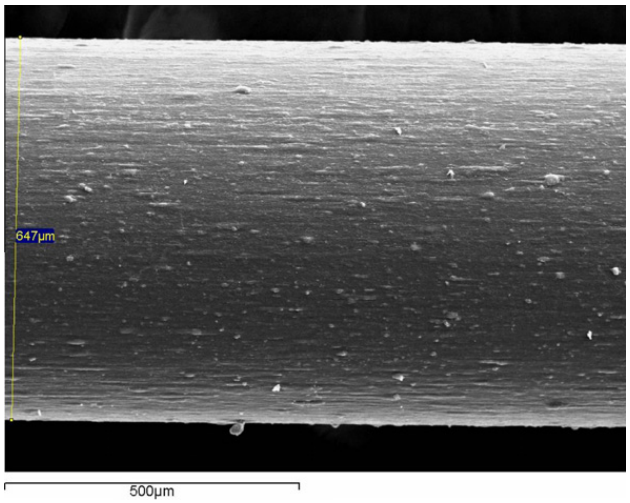

Fig. 7a. PU core.

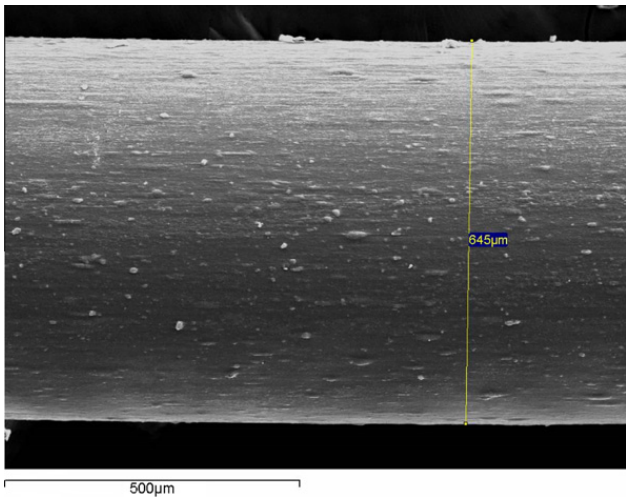

Fig. 7b. PU core.

Images acquired during the tensile test were processed to determine the gauge length and width for the core, wrap and yarn. The measured widths of the samples as a function of longitudinal strain are shown below in Fig. 9.

Using the gauge width, the engineering lateral strain was calculated, allowing the Poisson's ratio to be calculated.

Fig. 10 shows the Poisson's ratio as a function of the applied strain for both monofilament component fibres and their respective helical auxetic yarn. At low strains the polyamide wrap fibre exhibits a ν of approximately 2 which decreases to a magnitude in the region of 1 before failure. The polyurethane core fibre shows a measured ν in the range of 0.34–0.74 over a strain range 4 times that of the wrap. At low strains the core fibre demonstrates the highest value for ν which, as the applied strain is increased, diminishes linearly to its minimum value.

Combining these two monofilaments in a helical arrangement produces a markedly different behaviour in structural geometry as a function of applied strain. At strains below 0.02 we can observe a rapid increase in ν for the structure after which an equally sharp decrease in ν is shown. This is the onset of (true) auxetic behaviour. The yarn demonstrates engineering auxetic behaviour at 0.03ε when a negative ν is observed. The auxetic effect continues further as the strain is applied and a minimum value of ν at -2.79 is observed at a strain of 0.06. Continued application of strain produces a continued auxetic effect but decreasing in magnitude until failure of the wrap. As the yarn is extended the wrap fibre straightens before failing at a strain of 0.3, nearly twice the strain at failure observed for the wrap fibre alone. This behaviour of the HAY is characteristic to this particular material and geometry.

Plotting the yarn alone in Fig. 11 clearly shows the strain dependent behaviour of the yarn in addition to the experimental errors in calculating the Poisson's ratio.

The experimental error reduces as a function of the applied longitudinal strain due to the engineering strains used to calculate Poisson's ratio. We can show the sensitivity of the measurement system to only be valid for strains greater than 1% as below this value the error bars are unacceptably high. The data in Fig. 11 represents the greatest experimental error produced in this work as the images were obtained using the lowest pixel resolution. The experimental errors for calculating Poisson's ratio are shown for each data set as a percentage of the errors shown in Fig. 11.

Fig. 12 shows the effect of varying the angle of the wrap fibre on the auxetic effect of the yarn. The wrap fibre used was nominally 150 µm in diameter, giving a core to wrap diameter ratio of 4.2:1. The lowest starting angle of 13° corresponds to the data shown previously in Fig. 11. Increasing the starting angle to 22° shows similar low strain behaviour in the rapid increase and subsequent decrease in ν to a minimum value of -1.37. A change in starting angle of 9° produces nearly a 50% change in the auxetic effect of the yarn. The onset of auxetic behaviour is observed at a comparably low strain however true auxetic behaviour is observed at a marginally higher strain as the wrap fibre is not sufficiently straight to activate the core. The yarn with a 30° angle shows the initial positive increase in ν followed by a gradual decrease in magnitude to a strain of 0.3 where engineering auxetic behaviour of the order -0.06 is observed and maintained constant until failure of the wrap. With a 38° starting angle a low strain rapid increase in ν is observed, followed by a gradual increase in ν to 0.2ε, then a slow decrease to failure at 0.56ε. Engineering auxetic behaviour is not observed for this high starting angle and fibre geometry pair.

The ratio of core to wrap fibre diameters is the second geometric parameter we have used to tailor the auxetic effect. Fig. 13 shows the effect of changing the wrap diameter on the auxetic effect of the yarn. Three yarns were manufactured with an intended wrap angle of 30°; however variations in angle due to fibre relaxation and, predominantly, slip due to a low friction between the fibres resulted in a slight variation between yarns. The measured wrap angle for each yarn is stated in Fig. 13.

All three variations in wrap diameter show the initial increase in ν versus strain however this effect is most pronounced for the smallest diameter wrap fibre. Poisson's ra-

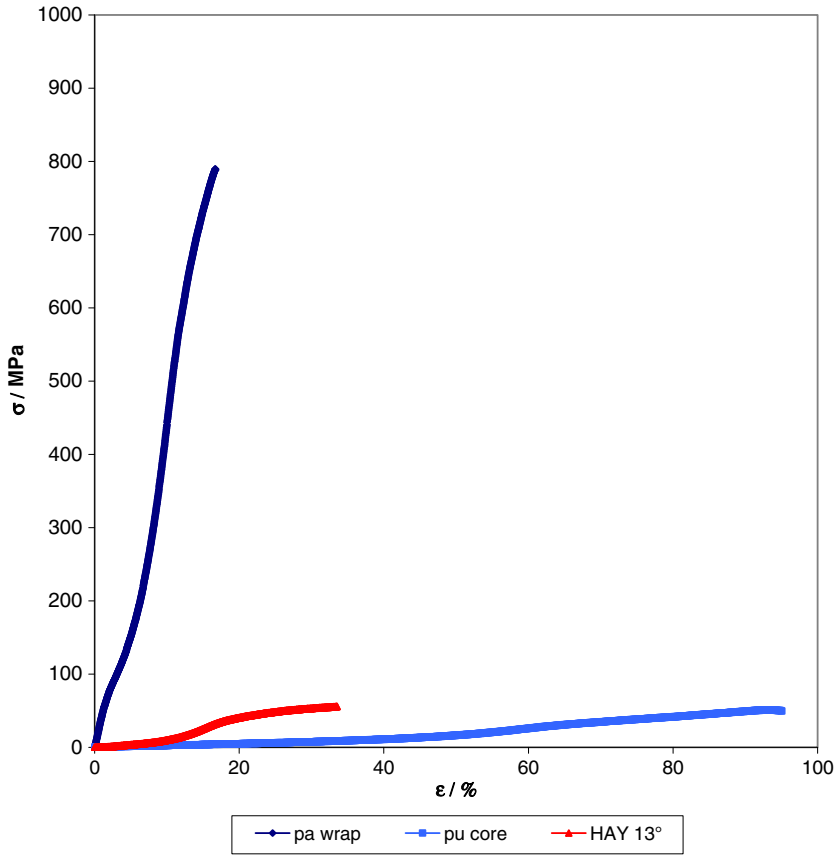

Fig. 8. Stress vs ε_{long} core, wrap and yarn.

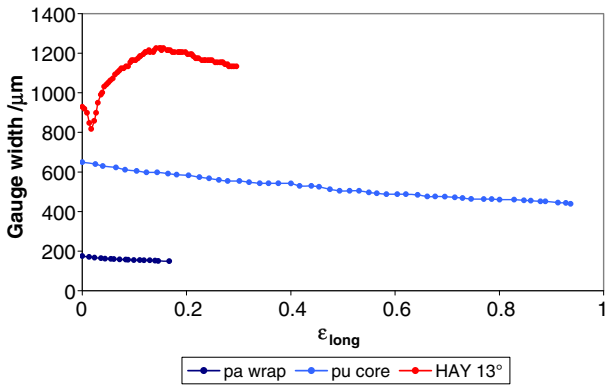

Fig. 9. Width vs ε_{long} core, wrap and yarn. Width Errors Yarn ±31 µm, Core ±25 µm, Wrap ±10 µm.

tio can then be observed to decrease in a steady manner for all fibres before tensile failure of the wrap. The only sample to show true auxetic behaviour incorporated the nominal 150 µm diameter fibre – the largest diameter of the three wraps.

All HAY's tested in this study failed due to fracture of the wrap fibre. Relative slip between core and wrap fibres was not observed for any HAY's during testing.

5. Discussion

Helical auxetic yarns manufactured and tested in this study have been shown to demonstrate Poisson's ratios as low as −2.7. The magnitude of v is dependent on yarn geometry – wrap fibre starting angle and diameter ratio – and the v of the component fibres. High resolution images of monofilament fibres obtained during tensile testing showed a high anisotropy in the polyamide wrap fibres as the calculated values extend beyond the range dictated by classical theory for isotropic materials of between 0 and 0.5. The polyurethane core fibres proved to be less anisotropic and demonstrated failure at much higher strains and as such lend themselves well as core fibres in HAYs.

A low and predictable Poisson's ratio is desirable for the core as any thinning of this fibre negates the auxetic effect achieved by the helical structure.

The majority of HAYs tested demonstrated a sharp increase in v at low strains before peaking and reducing in magnitude. We can attribute this behaviour to the internal helix diameter of the wrap fibre conforming to the unstrained diameter of the core and hence a rapid decrease in the net width of the yarn.

As the applied strain is increased the abrupt change in direction of v and equally rapid rate of decline is the result of activation of the core fibre into a helical form and the onset of engineering auxetic behaviour. It is therefore possible to remove the initial variation in v by pre-tensioning the yarns to a given strain. Once activated the core defines the net width of the structure and is responsible for the auxetic behaviour of the yarn until failure of the wrap fibre – at an applied strain dependent on the starting geometry

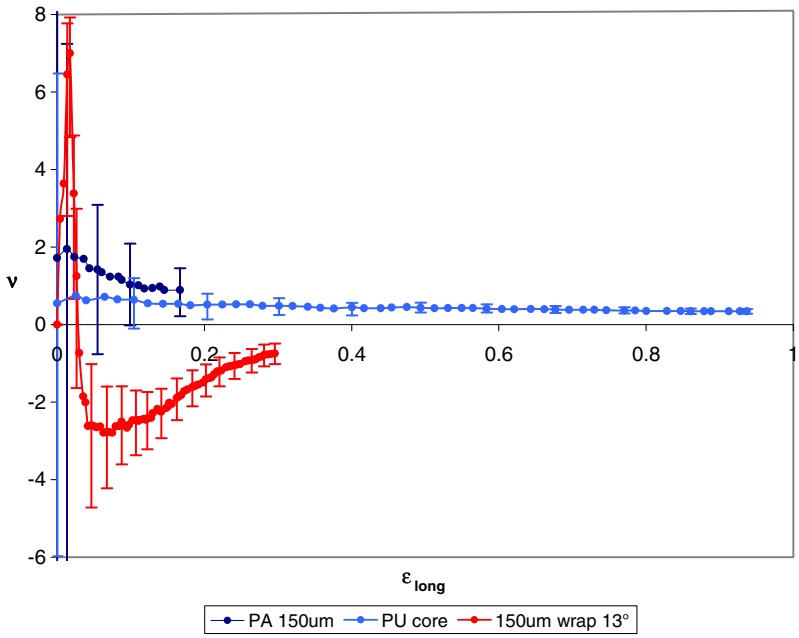

Fig. 10. v vs ε_{long} for monofilament component fibres and HAY.

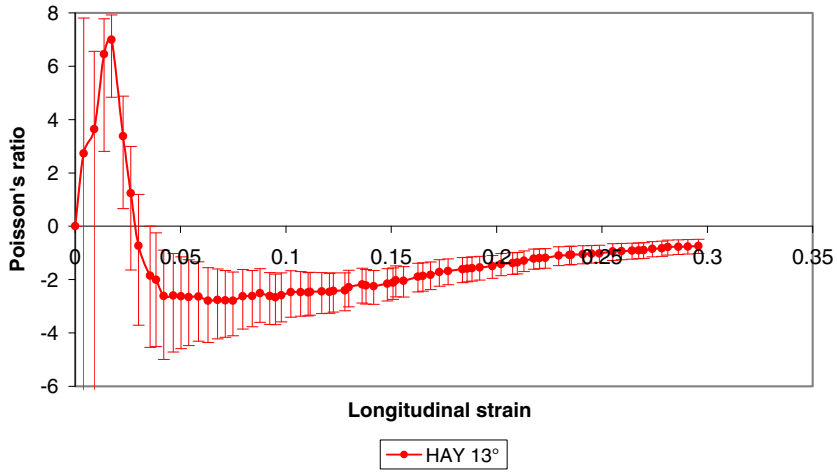

Fig. 11. v vs ε_{long} for HAY.

of the yarn. Relative slip between core and wrap fibres was not observed verifying a good conformance between the fibres. We would expect a degree of slip and frictional effects were this not the case, which in turn will reduce the geometric effect on the auxetic behaviour of the structure.

The transient nature of v as a function of applied strain for HAYs can be attributed to the competition between geometric and material effects of the yarn. Positive v values for the component fibres counteract the geometric effect from core activation. Depending on yarn geometry, this competition can be seen as either a gradual or near zero change over a given strain range.

For maximum auxetic effect, low strain activation of the yarn is desirable so that the geometric effect of the HAY is allowed to dominate over the material dependent behaviour of the component fibres. Early activation of the core is achieved by a low starting wrap angle and a high stiffness wrap. The stiffness of the wrap is both material and geometry dependent, i.e. a larger diameter wrap is structurally stiffer than a smaller diameter of identical material, a result confirmed by numerically modelling the mechanical behaviour of helical auxetic yarns (Wright et al., 2010). This conflicts with the desire to minimise the apparent width of the yarn at zero strain by employing a low diameter wrap fibre. Therefore, the greatest auxetic effect will be observed when a wrap fibre of infinitely low diameter and high stiffness is used.

We have shown that variation in zero strain wrap angle has a greater effect on the auxetic behaviour compared to the relative fibre diameters. This result is demonstrated by comparing the results in Figs. 12 and 13 highlighting the sensitivity of auxetic behaviour to starting wrap angle.

Variation in fibre diameter ratio showed less impact on the auxetic performance of a HAY compared to the wrap angle whilst highlighting the importance of wrap geometric stiffness. Modulus of the wrap material is important

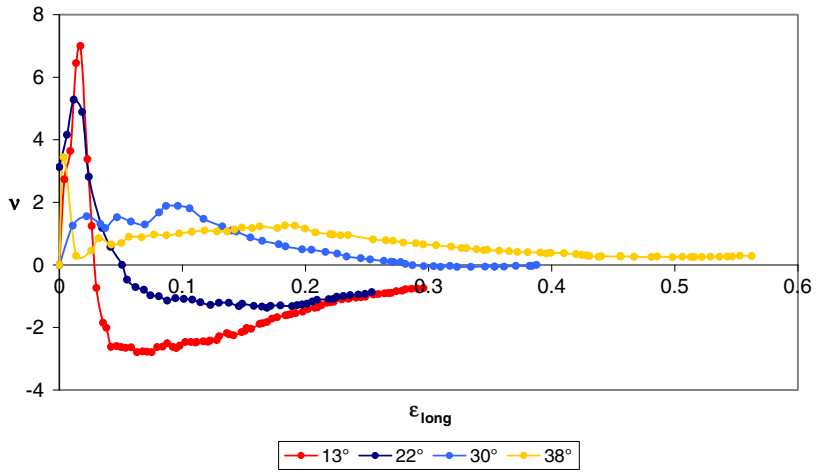

Fig. 12. Variation in wrap angle on auxetic performance of HAY. Error in Poisson's ratio measurement as a percentage of 13° yarn. 22° (86%), 30° (89%), 38° (75%).

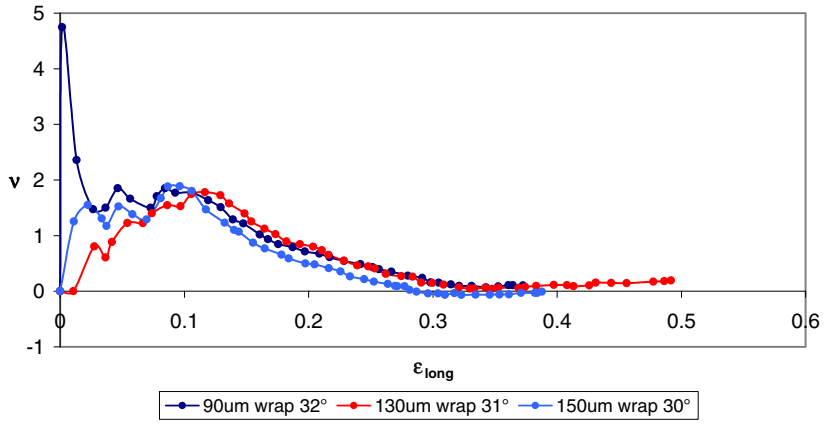

Fig. 13. Variation on fibre diameter ratio on auxetic performance of HAY. Error in Poisson's ratio measurement as a percentage of 13° yarn. 90 μm wrap 32° (65%), 130 μm wrap (70%), 150 μm wrap (75%).

however it is the stiffness of the fibre geometry that should be considered foremost.

Applications for auxetic textiles include shockwave protection fabrics – blast, flood, and storm – smart filters, composite reinforcement, body armour and geo-textiles.

6. Conclusions

Helical auxetic yarns using monofilament polymeric fibres have been defined, manufactured and characterised in this work. This work represents the first detailed, experimental study of the auxetic properties of simple HAYs. For these monofilament yarns the effect on ν as a function of applied strain and manufactured geometry has been discussed and the key geometric parameters used to tailor auxetic behaviour identified.

- Auxetic yarns have been accurately manufactured by spinning together two, commercially available, low cost fibres.
- The maximum auxetic effect observed for the yarns was −2.7, using monofilament fibres with Poisson's ratios ranging from 0.35 to 1.95.
- The starting angle of the wrap fibre dominates the magnitude of auxetic behaviour.
- The auxetic performance is also affected by the diameter ratio of wrap to core fibres and the inherent Poisson's ratio of the fibres.

Acknowledgements

The authors of this work would like to acknowledge the EPSRC for financial support and also the industrial collaborators – Auxetix Ltd., Monofil Trading Company Ltd, Home Office Scientific Development Branch, Centre for the Protection of National Infrastructure. We are very grateful for the assistance and skills of the staff at Exeter University, namely Peter Gerry, Mike Burns and Dave Baker.

Appendix A

The manufacture of helical auxetic yarns used a specially designed and manufactured spinner as shown in Fig. 14. Preparing the spinner for yarn manufacturer required loading core and wrap fibres onto spools 1 and 2

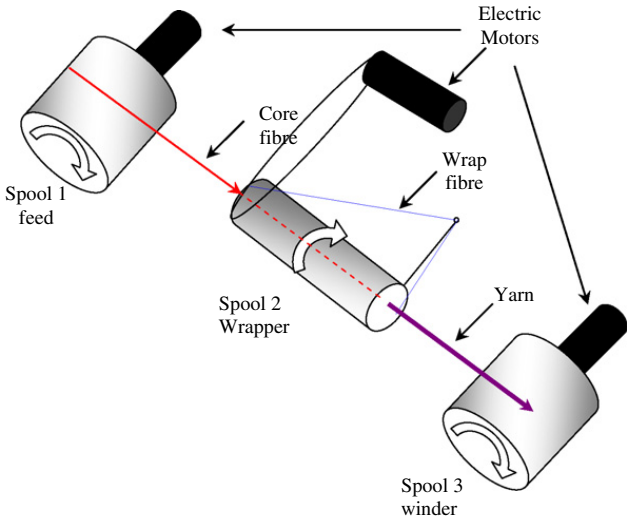

Fig. 14. Schematic of HAY yarn spinner.

respectively. Fibres were manually wound onto the spools to ensure an even lay of fibre under minimal tension. Rotation of the feed spool allowed the core to be threaded through the centre of spool 2 and then onto the winder spool 3. A number of eyelet guides and fibre tension either side of spool 2 gave both directional and tension control of the fibre. Stability of both these parameters is fundamental to accurate and consistent manufacture of helical auxetic yarns.

Handling elastomeric fibres has many inherent problems due to the low elastic modulus of the materials. Great care was taken throughout the spinning process to minimise the tension on both core and wrap fibres whilst retaining close control of the fibres. The elastomeric core was fed through the spinner at a constant linear feed rate by setting the feed and winder spools at equal speeds using electronic motor controllers. Fine tension adjustments to the core and wrap fibres were made using counterbalance weights and a simple brake mechanism of the respective feed spools. A line counter recorded the linear throughput of fibre.

Yarn geometry was controlled by adjusting the rotational speed of motors 1, 2 and 3 via an LCD control panel. Spools 1 and 3 dictated the linear speed and tension of the core fibre, spool 2 controlled the rotational frequency of the wrap fibre around the core. Empirical trials were employed to quantify these parameters with respect to the numerical values set on the motor control panel.

Figs. 15 and 16 show the numerical relationship between motor setting and linear core speed and wrap rotational frequency respectively.

The geometry of the yarns as previous defined is described in Eq. (6)

$$\lambda = \frac{\pi(D_c + D_w)}{\tan\theta} \tag{6}$$

where;

D_c = Diameter of core fibre (m)
D_w = Diameter of wrap fibre (m)
λ = Cyclic pitch of wrap fibre (m)

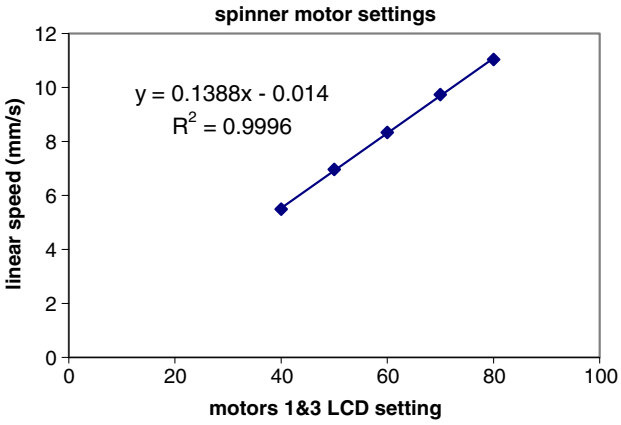

Fig. 15. Linear speed of core versus motors 1 and 3 control.

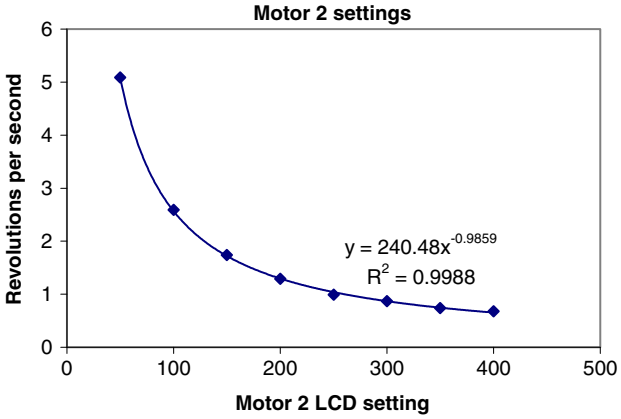

Fig. 16. Rotational frequency of wrap versus motor 2 control.

θ = Wrap angle (deg)

The linear feed rate of the core is taken from the numerical relationship calculated in Fig. 15.

Knowing the desired pitch length we can define the wrap frequency by dividing by the linear feed rate of the core fibre as defined by equation 7

$$f_w = \frac{v_c}{\lambda} \tag{7}$$

where;

f_w = Wrap frequency (s^{-1})
λ = Cyclic pitch of wrap fibre (m)
v_c = Linear feed rate of core fibre (ms^{-1})

Practically, it is desirable to set a high linear feed of the core fibre to enable a high throughput; however, in practice there is a compromise as lower speeds stabilise the process by minimising accumulated stretch in the elastomeric material. Once a stable linear feed of the core was established, the rotational frequency of the wrap was defined.

The wrap frequency can also be defined as a function of the rotational speed of motor 2 which has been calculated using Fig. 16 and is defined in equation 8.

$$f_w = 240.48 m_2^{-1} \tag{8}$$

where

f_w= Wrap frequency (s^{-1})

m_2 = motor 2 control setting (no units)

Equating (7) and (8) and solving for m_2 gives;

$$m_2 = \frac{240.48\, v_c}{\lambda} \tag{9}$$

Therefore, for a given fibre diameter pair and desired wrap angle, the pitch length can be defined using equation (1). The pitch length can therefore be combined with the chosen linear feed rate and used to calculate the motor control setting for the wrap fibre. For shallow wrap angles such as 10°, a high linear feed rate can be set as a low number of wrap fibre rotations per unit length are required. For steeper angles such as 40° low feed rates must be selected to minimise the rotational speed of the wrap fibre. Without a stable wrapping process, the manufactured yarns will display numerous geometric problems such as inconsistent wrap angle, poor wrap conformance with core, fibre twist and high fibre tension. The latter is the major cause of manufactured error as it causes relaxation – in the case of the core – and early activation of the yarn – in the case of the wrap.

Monofilament yarns show greatest stability when manufactured with wrap angles of 20° and above as the tightly wound spring nature of the higher angle wraps provide rigidity to the yarn both axially and in bending. The low coefficient of friction between the monofilament fibres is detrimental to the geometric stability of the yarns, especially at low wrap angles. Typical lengths of yarns manufactured using the spinner was approximately 10 meters at a time.

References

Abramoff, M.D., Magelhaes, P.J., Ram, S.J., 2004. Image Processing with ImageJ. Biophotonics International 11 (7), 36.

Alderson, K.L., Alderson, A., Webber, R.S., Evans, K.E., 1998. Evidence for uniaxial drawing in the fibrillated microstructure of auxetic microporous polymers. Journal of Material Science Letters 17, 1415–1419.

Alderson, K.L., Webber, R.S., Evans, K.E., 2000. Novel variations in the microstructure of the auxetic microporous ultra high weight polyethylene. Part 2. Mechanical Properties, Polymer Engineering and Science 40, 1906–1914.

ASTM. 2007. D 3822-07. Standard Test Method for Tensile Properties of Single Textile Fibers.

Baughman, R.H., Shacklette, J.M., Zakhidov, A.A., Stafstrom, S., 1998. Negative Poisson's ratios as a common feature of cubic materials. Nature 392, 362.

Caddock, B.D., Evans, K.E., 1989. Microporous materials with negative Poisson's ratios. 1. Microstructure and Mechanical Properties, Journal of Physics D: Applied Physics 22, 1877–1882.

Chan, N., Evans, K.E., 1997. Fabrication methods for auxetic foams. Journal of Materials Science 32, 5945–5953.

Chan, N., Evans, K.E., 1998. Indentation resilience of conventional and auxetic foams. Journal of Cellular Plastics 34, 231–260.

Evans, K.E., Alderson, A., 2000. Auxetic materials: Functional materials and structures from lateral thinking. Advanced Materials 12 (9), 617–628.

Evans, K.E., Nkansah, M.A., Hutchinson, I.J., Rogers, S.C., 1991. Molecular network design. Nature 353, 124.

Evans, K.E., Donoghue, J.P., Alderson, K.L., 2004. The design, matching and manufacture of auxetic carbon fibre laminates. Journal of Composite Materials 38 (2), 95–106.

Frohlich, L.M., Labarbera, M., Stevens, W.P., 1994. Poisson's ratio of a crossed fibre sheath: the skin of aquatic salamanders. Journal of Zoology London 232, 231–252.

Gaspar, N., Ren, X.J., Smith, C.W., Grima, J.N., Evans, K.E., 2005. Novel honeycombs with auxetic behaviour. Acta Materialia 53, 2439–2445.

Gunton, D.J., Saunders, G.A., 1972. The Young's modulus and Poisson's ratio or arsenic, antimony and bismuth. Journal of Materials Science 7, 1061–1068.

Hall, L.J., Coluci, V.R., Galvao, D.S., Kozlov, M.E., Zhang, M., Dantes, S.O., Baughman, R.H., 2008. Sign change of Poisson's ratio for carbon nanotube sheets. Science 320, 504.

Hilton, H.H., Lee, D.H., El Fouly, A.R.A., 2008. Generalized viscoelastic designer functionally graded auxetic materials engineered/tailored for specific task performances. Mechanics of Time-Dependent Materials 12, 151–178.

Hook, P.B., Evans, K.E., Hannington, J.P., Hartmann-Thompson, C., Bunce, T.R., 2006. Patent number: KR20060009826.

Kocer, C., McKenzie, D.R., Bilek, M.M., 2009. Elastic properties of a material composed of alternating layers of negative and positive Poisson's ratio. Materials Science and Engineering A505, 111–115.

Lakes, R.S., 1987. Foam structure with a negative Poisson's ratio. Science 235, 1038.

Lees, C., Vincent, J.E.V., Hillerton, J.E., 1991. Poisson's ratio in skin. Biomedical Materials and Engineering 1, 19–23.

Miller, W., Hook, P.B., Smith, C.W., Wang, X., Evans, K.E., 2009. The manufacture and characterisation of a novel, low modulus, negative Poisson's ratio composite. Composites Science and Technology 69 (5), 651–655.

Pickles, A.P., Alderson, K.L., Evans, K.E., 1996. The effects of powder morphology on the processing of auxetic polypropylene. Polymer Engineering and Science 36 (5), 636–642.

Ravirala, N., Alderson, A., Alderson, K.L., Davis, P.J., 2005. Expanding the range of auxetic products using a novel melt spinning route. Physica Status Solidi B 242 (3), 653–664.

Shanahan, M.E.R., Piccirelli, N., 2008. Elastic behaviour of a stretched woven cloth. Composites Part A Applied Science and Manufacturing 39, 1059–1064.

Theiocaris, P.S., Stavroulakis, G.E., Panagiotopoulos, P.D., 1997. Negative Poisson's ratios in composites with star shaped inclusions: a numerical homogenization approach. Archive of Applied Mechanics 67, 274–286.

Ugbolue, S.C, Warner, S.B., Kim, Y.K., Fan, Q., Yang, C.L., Kyzymchuk, O., Feng, Y., 2007. The formation and performance of auxetic textiles, Report, National textile centre, USA, NTC project: F06-MD09, pp. 1–10.

Williams, J.L., Lewis, J.L., 1982. Properties and an anisotropic model of cancellous bone from the proximal tibial epiphysis. Trans. ASME, Journal of Biomechanical Engineering 104, 5–56.

Williams, J.J., Smith, C.W., Evans, K.E., Lethbridge, Z.A.D., Walton, R.I., 2007. An analytical model for producing negative Poisson's ratios and its application in explaining off-axis elastic properties of the NAT-type zeolites. Acta Materialia 55 (17), 5697–5707.

Wright, J.R., Sloan, M.R., Evans, K.E., 2010. Novel tensile properties of helical auxetic structures: a numerical Study. Journal of Applied Physics 108, 044905.